Analytical and Bioanalytical Chemistry
https://doi.org/10.1007/s00216-025-06309-w

RESEARCH PAPER

Automated methods for multi-isotopic analysis of major cations in biological samples: application to chronic kidney disease of unknown etiology

Rosa Grigoryan[1,2] · William Swenson[3] · M. Paul Field[3] · Mangala Chatura De Silva[4] · Anna Strasma[5] · Nishad Jayasundara[5,6] · Michael A. Kipp[1]

Received: 29 August 2025 / Revised: 18 December 2025 / Accepted: 23 December 2025

Abstract

Natural variability in stable isotope ratios provides critical constraints on elemental cycling in nature without the need for the introduction of artificial tracers. While such data are widely used in environmental studies, they are not as widely employed in biomedical research, despite vast potential. One critical hurdle to the adoption of such techniques in biomedical studies is sample throughput. Elemental purification via ion-exchange chromatography and isotopic analysis via multiple collector inductively coupled plasma mass spectrometry (MC-ICP-MS) are time-consuming, requiring long hours from experienced researchers to generate datasets. Here we present new methods to improve the throughput of both elemental purification and sample introduction to mass spectrometers. We use an automated, low-pressure ion exchange chromatography system to isolate purified fractions of potassium, magnesium, and calcium from one sample in a single sequence with high yields (80–100%) and low blanks (<0.5% carryover). Modification of flow rates and column volumes also enables recovery of purified strontium, lithium, and sodium in the same routine. Solutions are introduced to the MC-ICP-MS via syringe injection and with automated removal of vial caps to minimize evaporation. We find that syringe injection from capped vials gives a > 10 × more stable signal (0.7% RSD) over a 9-h sequence than self-aspirated, uncapped solutions (8.0% RSD). Syringe injection also enables modification of signal intensity by changing the injection rate, with a linear response of signal to flow rate. We demonstrate the potential of these methods by analyzing calcium, magnesium, and potassium isotope ratios at high precision (<0.1 ‰) from single 0.5 mL aliquots of urine samples from individuals with chronic kidney disease. These data show a change in calcium reabsorption, highlighting avenues for further research as well as the value of these multi-isotopic analysis methods.

Keywords Chromatography · Spectrometry · Calcium · Magnesium · Potassium

Introduction

The relative abundance of stable isotopes provides information about the sources and chemical transformations of elements in nature [1]. Isotope ratio analyses have thus been leveraged to constrain elemental fluxes at scales ranging from the Earth and Moon [2, 3] to the critical zone [4], biological tissues [5, 6] and even individual molecules [7, 8]. Despite the broad utility of isotope ratio analysis, applications of this technique remain hindered by slow sample

✉ Rosa Grigoryan
rosa.grigoryan@duke.edu

✉ Michael A. Kipp
michael.kipp@duke.edu

[1] Division of Earth and Climate Sciences, Nicholas School of the Environment, Duke University, Durham, NC, USA

[2] Shared Materials Instrumentation Facility, Pratt School of Engineering, Duke University, Durham, NC, USA

[3] Elemental Scientific Inc., Omaha, NE, USA

[4] Department of Zoology, University of Ruhuna, Matara, Sri Lanka

[5] Division of Nephrology, Department of Medicine, Duke University School of Medicine, Durham, NC, USA

[6] Division of Environmental Natural Sciences, Nicholas School of the Environment, Duke University, Durham, NC, USA

Published online: 14 January 2026

throughput. This is particularly pronounced for so-called non-traditional stable isotope analysis (i.e., all elements except for H, O, C, N, S), which require tedious chromatographic purification prior to isotopic analysis. The rate of sample throughput thus limits the statistical power of non-traditional isotope reconstructions of element cycling in the environment, and furthermore stifles the exploration of isotope ratio analysis in other disciplines, such as medicine.

Since the advent of non-traditional isotope analysis by multiple collector inductively coupled plasma mass spectrometry (MC-ICP-MS) in the 1990 s, several studies have aimed to improve analytical throughput. These include efforts to scale up sample digestion [9, 10], automate ion-exchange chromatography [11], and optimize sample introduction to the mass spectrometer [12]. While these approaches have considerably diminished the time and effort required for isotope analyses via MC-ICP-MS, at present it is still the norm to conduct single-element studies due to the need to individually tailor purification and measurement techniques on a per-element basis. This leaves the field with a narrow view of the drivers of isotopic variability since inter-element correlations are rarely explored in detail.

Here we present new methods that overcome some of these obstacles. We developed an ion-exchange chromatography method that enables purification of multiple elements (lithium, sodium, potassium, magnesium, strontium, calcium) in a single 3-h sequence. This method is potentially applicable to a wide range of sample matrices (e.g., urine, seawater, mineral digests). We furthermore improved the precision of isotopic analysis via MC-ICP-MS by using a syringe injection system to introduce sample solutions to the plasma. This has the benefit of superior stability compared to self-aspirating nebulization, and also allows modification of syringe injection rates to achieve precise sample-standard intensity matching. Collectively, these improvements make it much more feasible to obtain large, high-precision, multi-isotopic datasets.

We demonstrate the potential of these new methods by analyzing the Ca, Mg, and K isotopic composition of urine samples from individuals with a unique form of chronic kidney disease (CKD) associated with environmental causes termed CKD of unknown etiology (CKDu). Prior work has identified isotopic fractionation during renal reabsorption of Ca [13]. Such data do not exist for Mg and K in human urine, though animal models suggest moderate and small isotopic effects for Mg [14] and K [15], respectively. In theory, changes in fractional ion reabsorption in the nephron should result in detectable isotopic variations in urine. In the best case, multi-element (Ca, Mg, K) isotopic datasets could identify site-specific renal dysfunction, since the relative reabsorption of each ion varies throughout the nephron [16]. Our data reveal systematic changes in ion reabsorption and calcium isotope fractionation between healthy and CKDu populations, highlighting the potential of these analyses to quantify renal ion reabsorption, with possible applications for distinguishing the progression of CKDu versus CKD from traditional causes such as diabetes and hypertension.

Experimental

Reagents and materials

All lab work was conducted in GAIA Lab (Geoscience Applications of Isotopic Analysis) in the Division of Earth and Climate Sciences at Duke University and the Duke University Shared Materials Instrumentation Facility (SMIF).

Ultrapure water with 18.2 MΩ cm resistivity obtained from a Milli-Q IQ7000 water purification system (Millipore Sigma) was used throughout this study. Unless otherwise specified, all acids were twice-distilled from ACS reagent grade acid using Analab CleanAcids sub-boiling purification systems (ESI, Omaha, NE) or purchased as Optima grade (Fisher Chemical). Optima grade hydrogen peroxide (31%) was obtained from Fisher Chemical. Perfluoro alkoxy (PFA) polymer vials were obtained from Savillex and Elemental Scientific.

Ca SPEX CertiPrep (lot # CL15-24CAY), Mg SPEX CertiPrep (lot # 27-194MGY), and NIST 999c potassium chloride were used as bracketing standards for calcium, magnesium, and potassium isotope ratio measurements, respectively. NIST SRM 1486 Bone meal, ERM AR-143, IAPSO seawater (SW) (batch # P168), human pooled urine (Innovative Research Inc., batch # 53979) standards were used as secondary reference materials for quality control.

Urine samples for the present study were collected from Matara, a CKDu nonendemic region, where CKDu has not been reported, and Padaviya, a CKDu endemic region in Sri Lanka. Samples were collected from CKDu patients from the endemic region without a diagnosis of hypertension and diabetes and registered at a government clinic for CKDu treatment. Healthy individuals who were not diagnosed with any form of kidney disease from the non-endemic region served as the control group. Demographic data, medical history, lifestyle habits, family history of diseases, current health status, water source, and occupational/farming characteristics were obtained from an interviewer-administered structured questionnaire as previously described [17]. Each individual provided a midstream first void (morning) urine sample in a 50-mL urine collection tube containing Norgen urine preservative (Norgen Biotek, Thorold, ON, Canada). Samples were kept at room temperature according to the manufacturer's instructions and were stored at Duke University until analysis.

Sample purification

Sample preparation was carried out in a metal-free clean lab environment. Urine samples containing visible red blood cells were excluded due to differences in the Ca isotopic signature of urine and blood [18]. Urine samples (300–500 µL) were digested twice using 1 mL concentrated HNO_3 and 1 mL 31% H_2O_2 (v/v) in capped PFA vials at 120 °C overnight. The sample digests were evaporated to dryness and redissolved in 2 mL 0.5 M HNO_3 for elemental quantification (1 mL) and chemical purification (1 mL).

Sequential K, Mg, and Ca separations from the matrix were performed using two inline columns (C1 and C2; Fig. 1) on a prep*FAST* MC (ESI, Omaha, NE, USA) automated low-pressure chromatographic system. K and Mg were purified using column 1 (C1), loaded with 3 mL of AG50W-X8 resin (100–200 mesh, Bio-Rad), followed by Ca purification with column 2 (C2), loaded with 1 mL of DGA resin (50–100 µm, Eichrom). To monitor analyte recovery and sample-to-sample carryover, the IAPSO seawater reference material and procedural blanks were run at the beginning and end of each sequence. During the course of this method testing, both resins were successfully reused up to 100 times. A description of the separation protocol is presented in Table 1.

After both columns are cleaned and conditioned for the entire purification process, the sample is loaded onto C1 in 0.5 M HNO3 (Fig. 1B). The first step is to remove Na, Li, and B from C1 using 0.5 M HNO_3. Following the removal of these elements, K is isolated with an additional 0.5 M HNO_3. This is followed by 1 M HNO_3 in order to fully elute Mg. With Sr and Ca still bonded to C1, C2 becomes an active column in the flow path. Both analytes are transferred to C2 via 2 M HNO_3 (Fig. 1D). C1 is deactivated, and Sr is eluted from C2 with 6 M HNO_3 (Fig. 1C). Finally, 0.1 M HCl is eluted through C2 to isolate Ca. An elution curve was established using a synthetic inorganic urine solution mimicking the major ion content of Seronorm urine standard (Table 2). This curve was generated via a column calibration performed at Elemental Scientific (described in Mass spectrometry).

Purified K, Mg, and Ca fractions were evaporated to dryness and redissolved in concentrated HNO_3 (1 mL) and 31% H_2O_2 (0.5 mL). The solutions were heated in closed vials at 120 °C overnight to remove organic compounds from the resin. This procedure was performed twice, followed by drying at 90 °C and redissolution in 1 mL 2% HNO_3 (v/v) for isotope ratio measurements.

Table 1 Multi-element purification method

Method Step	Reagent	Volume (mL)	Flow Rate (mL/min)
Clean C1 + C2	6 M HNO_3	15	5
Clean C1	MQ H_2O	15	5
Condition C1	0.5 M HNO_3	6	5
Sample Load C1	0.5 M HNO_3	1	1
Wash matrix C1 (Li, Na)	0.5 M HNO_3	25	1
Elute K C1	0.5 M HNO_3	18	1
Wash matrix C1	0.5 M HNO_3	15	1
Wash matrix C1	1 M HNO_3	10	1
Elute Mg C1	1 M HNO_3	28	1
Transfer Wash C2	2 M HNO_3	20	3
Elute Sr C2	6 M HNO_3	8	1
Elute Ca C2	0.1 M HCl	6	3
Wash matrix C2	0.1 M HCl	3	4
Wash matrix C2	MQ H_2O	3	1

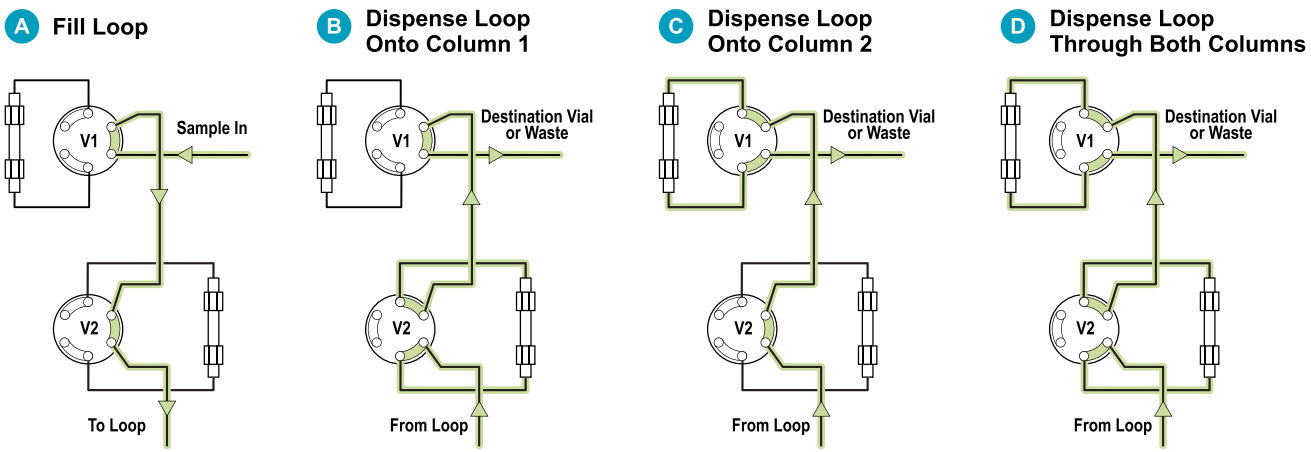

Fig. 1 Schematic of two-column plumbing. Four operational modes are available: **A** loading solution into the loop, **B** dispensing solution through column 1, **C** dispensing solution through column 2, **D** dispensing solution through both columns

Table 2 Multi-element synthetic urine solution composition. Single-element ICP solutions were used to produce an inorganic synthetic urine solution to calibrate the column yields

Element	Urine
Ca	71 mg L^{-1}
Cu	31 µg L^{-1}
Fe	13.7 µg L^{-1}
Li	7 µg L^{-1}
K	1495 mg L^{-1}
Na	2287 mg L^{-1}
Sr	89 µg L^{-1}
Zn	334 µg L^{-1}
Mg	64 mg L^{-1}

Sample introduction

The micro*FAST* isotope 2 is a dual-loop, syringe-driven, valve injection system for plasma-based mass spectrometers. The system uses software control to automatically syringe load and syringe inject Loop 1 at user-defined flow rates (10–300 µL/min) while rinsing the sample probe and Loop 2 in preparation for the next sample. The valve can select from two discrete parallel flow paths (loop 1 or loop 2), allowing for rapid switching between samples with minimal dead volume [19]. To maintain sample/standard/blank integrity, the isotope 2 is equipped with a fluoropolymer-coated autosampler arm attachment. This attachment is pneumatically operated and automatically removes and replaces covers on sample containers at the time of analysis, minimizing contamination and evaporation of samples during extended analytical sessions.

Mass spectrometry

Column calibration was performed via ICP-MS (Agilent 7900) and ICP-OES (Thermo Fisher iCAP PRO) analysis at Elemental Scientific. Acid increments of 1 mL were passed through the prepFAST and subsequently diluted with MQ H_2O to a volume of 10 mL before being administered via an autosampler to the ICP-MS and ICP-OES. The Agilent 7900 ICP-MS was operated at an RF Power of 1550 W with platinum skimmer and sample cones and a quartz torch and spray chamber. The iCAP PRO ICP-OES was operated at an RF Power of 1250 W with EMT DUO quartz torch. Each ICP-MS run monitored ^{7}Li, ^{24}Mg, and ^{88}Sr, and each ICP-OES run monitored Ca, Na, and K to quantify elemental abundances. Reproducibility, assessed as the variance of replicate analyses of 1 mL 0.5 M HNO_3 passed through the column, was < 5% RSD for ICP-MS and < 3% RSD for ICP-OES.

Major element concentrations (Mg, Ca, K, Na) in urine samples were measured via inductively coupled plasma mass spectrometry (ICP-MS, Thermo Fisher X-Series II) at Duke University following published protocols [20]. Aliquots of bulk digests were diluted in 0.3 M HNO_3 and bracketed by multi-element ICP standard solutions. We note that to avoid interferences that would compromise calculations of Ca concentrations using the ^{48}Ca signal, P and Ti were omitted from the multi-element standard. Reproducibility and instrument drift were monitored via replicate analyses of multi-element standards through an analytical sequence as well as repeat preparations and analyses of standard materials. External reproducibility for all analytes was < 10% RSD.

Mg, K, and Ca isotopic compositions were measured using a Nu Sapphire dual path collision/reaction cell-equipped multi-collector inductively coupled plasma mass spectrometer (CRC-MC-ICP-MS, Nu Instruments, UK). This instrument houses one ion-counting detector and sixteen Faraday cups with optional switchable resistors: one 10^{10} Ω, sixteen 10^{11} Ω, and fifteen 10^{12} Ω. It features a dual ion path—high energy (HE) and low energy (LE)—with acceleration voltages of 6 kV and 4 kV, respectively. The LE path houses a hexapole collision/reaction cell which allows removal of interfering species. A combination of Ni dry plasma cones and a desolvating nebulizer (Apex Ω HF; ESI, Omaha, NE, USA) was used to ensure high sensitivity. Typical instrument tuning settings are provided in Table 3.

Mg isotope ratios were measured in the HE path at medium (pseudo) mass resolution using four Faraday collectors connected to 10^{11} Ω amplifiers to monitor masses 23 through 26. Mg was measured at the left side of the peak center to ensure an interference-free signal from isobaric polyatomic ions, such as C_2^+, C_2H^+, $C_2H_2^+$, CN^+, and NaH^+. Mg isotope ratio measurements were performed on 100 µg L^{-1} solutions with a typical signal intensity of 37 V for total Mg. For all analyses performed here, on-peak zeroes were observed and either subtracted from sample and standard beam intensities or neglected if contributions were negligible.

Ca isotope ratios were measured in the HE path at medium (pseudo) mass resolution using four Faraday collectors connected to 10^{11} Ω amplifiers to monitor masses 42, 43, and 44, and a 10^{12} Ω amplifier for monitoring mass 43.5 ($^{87}Sr^{2+}$). Ca was measured in 2 mg L^{-1} solutions on the left side of the interference-free peak plateau to resolve polyatomic interferences (ArH_2^+, CO_2^+, N_3^+, N_2O^+). A first-order correction was performed by subtracting on-peak zero intensities, followed by a doubly charged Sr correction using the exponential law for instrumental mass bias.

K isotope measurements were conducted using the LE path at low mass resolution using three Faraday collectors all connected to 10^{11} Ω amplifiers to monitor masses 39, 40, and 41. The Ar^+ and ArH^+ species were removed via charge exchange reactions using H_2 gas and He buffer gas for collisional focusing [21]. Purified K was introduced into plasma in 30–40 µg L^{-1} solutions (yielding sensitivity of 1000 V ppm^{-1}).

Table 3 Instrument settings and data acquisition parameters for the Sapphire MC-ICP-MS. An automatic 2SD outlier rejection was applied to isotope ratio data by the instrument software

Instrumental settings					
RF power		1300 W			
Gas flow rates					
	Cool	13 L min^{-1}			
	Auxiliary	0.8 – 0.95 L min^{-1}			
	Nebulizer	30 – 33 psi			
Sampler cone		Ni sample cone: 0.9 mm aperture ⌀			
Skimmer cone		Ni skimmer cone: 0.7 mm aperture ⌀			
Nebulizer		Concentric, 100 µL min^{-1}			
Mass resolution mode		Low (K), medium (Ca, Mg)			
Data acquisition					
Integration time, sec		4			
Number of cycles		50			
Blocks		1			
Desolvating system					
Type		Apex Ω HF			
Ar sweep gas, L min^{-1}					
	Ca	1.75 – 2.3			
	K	2.1 – 2.4			
	Mg	2.6 – 3			
N_2 Additional gas, mL min^{-1}	Ca	10			
	K	5			
	Mg	0			
Spray chamber T, °C		140			
Peltier T, °C		3			
Oven T, °C		155			
Cup configurations					
Cup		L4	Ax	H2	H4
Resistor (Ω)		10^{11}	10^{11}	10^{12}	10^{11}
Isotope/mass	Ca	^{42}Ca	^{43}Ca	43.5	^{44}Ca
Cup		L4	Ax	H4	
Resistor (Ω)		10^{11}	10^{11}	10^{11}	
Isotope/mass	K	^{39} K	^{40} K	^{41} K	
Cup		L7	L4	H1	H5
Resistor (Ω)		10^{11}	10^{11}	10^{11}	10^{11}

Table 3 (continued)

Isotope/mass	Mg	^{23}Na	^{24} Mg	^{25} Mg	^{26} Mg
Lenses HE path					
Acceleration	Ca, Mg	6000 V			
Extraction	Ca, Mg	3300-4400 V			
Collision/reaction cell (LE path) for K measurement					
RF ref	− 9 to − 5				
Cell deceleration	− 51 to − 47				
Cell extraction	1.65 to 2				
Cell He gas flow (sccm)	5.0 to 5.2				
Cell H2 gas flow (sccm)	4.0 to 4.2				
Acceleration	4000 V				
Extraction	2000–2450 V				

Data reduction

All isotopic ratios are reported in delta notation (per mil, ‰) using standard-sample bracketing (SSB) for instrumental mass bias correction. The Mg isotopic composition was measured against Mg SPEX and determined using the equation:

$$\delta^{26}Mg\ (‰) = [(^{26}Mg/^{24}Mg)_{sample}/(^{26}Mg/^{24}Mg)_{standard} - 1] \times 1000 \quad (1)$$

ERM AE-143 was measured against the Mg SPEX solution during multiple sessions over a period of 6 months and has an identical isotopic composition ($\delta^{26}Mg_{Mg\ SPEX} = 0.00 \pm 0.02$ ‰, $\delta^{25}Mg_{Mg\ SPEX} = 0.00 \pm 0.02$ ‰, 2SE, $N = 9$). The measured data are therefore reported relative to ERM AE-143 for comparison with literature data.

Potassium isotopic ratios were measured and reported against the NIST SRM 999c primary standard, which is isotopically indistinguishable from NIST SRM 3141a [22, 23]:

$$\delta^{41}K\ (‰) = [(^{41}K/^{39}K)_{sample}/(^{41}K/^{39}K)_{SRM\ 999c} - 1] \times 1000 \quad (2)$$

Calcium isotope ratios were measured against the Ca SPEX CertiPrep elemental standard:

$$\delta^{44/42}Ca\ (‰) = [(^{44}Ca/^{42}Ca)_{sample}/(^{44}Ca/^{42}Ca)_{standard} - 1] \times 1000 \quad (3)$$

Two replicates of IAPSO seawater standard were included in each batch of purification chemistry and isotope ratio measurements. Following prior work [24], the sample $\delta^{44/42}Ca$ data were normalized to seawater using those replicate analyses of the IAPSO standard. The final values were then reported as $\delta^{44/40}Ca_{SW}$ assuming kinetic mass-dependent isotopic fractionation [25]:

$$\delta^{44/40}Ca = \delta^{44/42}Ca \times 2.05 \quad (4)$$

We note that if equilibrium rather than kinetic isotope fractionation is assumed, a conversion factor of 2.10 would apply rather than 2.05; considering that our average external reproducibility on $\delta^{44/40}Ca$ measurements is 0.09 ‰ and we are studying effects of > 1 ‰, the error from the incorrect choice of fractionation law will not significantly affect our conclusions. We favor the reporting of Ca isotope data relative to seawater because (i) certified reference materials NIST SRM 915a and 915b are not readily available, (ii) seawater is isotopically homogenous, abundant and affordable, and (iii) processing the reference material through each batch of chemical purification removes the potential for systematic matrix effects when normalizing samples to matrix-free standards.

Results and discussion

Multi-element purification

One goal of this study was the development and validation of an efficient purification procedure for target elements (Mg, K, and Ca) in urine samples while maintaining low procedural blanks and obtaining accurate isotope ratio values. While prior work has successfully implemented automated chromatography systems for generating large isotopic datasets [11, 18, 26, 27], such approaches have not been adapted to strategic multi-element combinations that would enable greater scientific insight with less sample processing time. Multi-element purification was achieved here by using a dual-column method in the prepFAST MC. Mg and K purifications were performed using 3 mL AG 50W-X8 resin followed by sequential purification of Ca from matrix with 1 mL DGA resin. Figure 2 shows the elution profile obtained for synthetic urine samples. Li (96.9%) and Na (99.8%) were efficiently removed using 25 mL 0.5 M HNO_3 (Table 1). K was collected with 18 mL 0.5 M HNO_3, followed by matrix washes with 18 mL 0.5 M HNO_3 and 10 mL 1 M HNO_3. Mg was collected with 28 mL 1 M HNO_3, followed by transfer of analytes to the second column by 2 M HNO_3. Sr was then removed with 8 mL 6 M HNO_3 and Ca was collected using 6 mL 0.1 M HCl, followed by column washes with 3 mL 0.1 M HCl and 3 mL MQ water. We note that in our method, Cu, Fe, and Zn will co-elute (> 99%) with the Mg fraction; however, the Cu/Mg, Fe/Mg, and Zn/Mg elemental ratios in urine samples are < 0.006. At these levels, $\delta^{26}Mg$ values are not impacted by matrix effects and do not exhibit any measurable bias [14].

Each batch of chemical purification included two procedural blanks (quantified via MC-ICP-MS) and two standards (one IAPSO SW in the beginning and another at the end of the sequence). NIST SRM 1486 RM was purified only for the Ca fraction. Procedural blanks ranged from 0.6–11 ng for

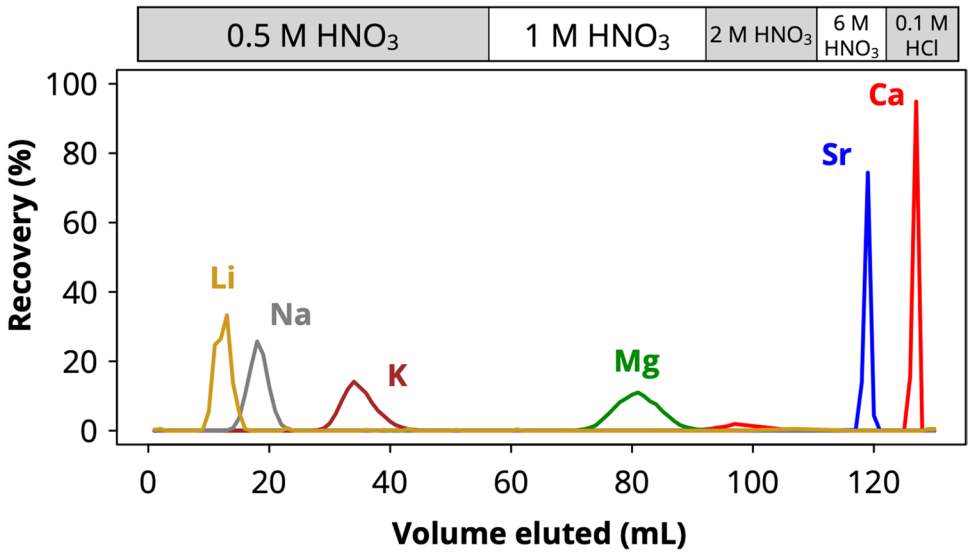

Fig. 2 Elution curve. Relative elemental recoveries are shown for a synthetic urine solution

Table 4 Isotopic standard data. Uncertainties are two times the standard error of the mean. *N* refers to the number of separate isolation replicates

Standard	$\delta^{41/39}K_{SRM\ 999c}$ (‰)	$\delta^{26/24}Mg_{ERM\ AE\text{-}143}$ (‰)	$\delta^{44/40}Ca_{SW}$ (‰)
IAPSO SW	0.05 ± 0.05 (2SE, *N* = 10)	2.39 ± 0.06 (2SE, *N* = 11)	0.00 ± 0.08 (2SE, *N* = 9)
NIST SRM 1486	-	-	− 3.06 ± 0.13 (2SE, *N* = 7)
Urine	− 0.48 ± 0.03 (2SE, *N* = 10)	3.10 ± 0.05 (2SE, *N* = 10)	− 1.10 ± 0.09 (2SE, *N* = 10)

Mg, 4–28 ng for K, and 42–108 ng for Ca, which are negligible compared to the amounts of these analytes recovered from typical urine samples (~ 30 µg, ~ 750 µg, and ~ 35 µg, respectively).

Table 4 presents the isotopic composition data for potassium ($\delta^{41}K$), magnesium ($\delta^{26}Mg$), and calcium ($\delta^{44}Ca$) across three different standards: IAPSO seawater (SW), NIST SRM 1486 bone meal, and pooled human urine. The $\delta^{41}K$ value for IAPSO seawater measured against NIST 999c was + 0.05 ± 0.05 ‰ (2SE, $N = 10$, where 2SE is the two times the standard error of the mean, $2*SD/\sqrt{n}$), which is in good agreement with the range reported in the literature (+ 0.03 to + 0.14 ‰) [e.g., 16]. The $\delta^{26}Mg$ value of IAPSO seawater measured against ERM AE 143 was + 2.39 ± 0.06‰ (2SE, $N = 11$), or − 0.91‰ when converted to the DSM3 scale, which is within the error margins reported in the literature (− 0.83 ± 0.11‰ [28]). The difference in $\delta^{44/42}Ca$ values between IAPSO SW and NIST SRM 1486 was − 1.45 ± 0.09‰ (2SE), which is in agreement with the literature value − 1.41 ± 0.05‰ [29]. Although $\delta^{44/42}Ca$ values were measured against the Ca SPEX elemental standard, the data are reported relative to IAPSO SW and expressed as $\delta^{44/40}Ca$ to allow better comparability with published Ca isotope data.

Reproducibility of Ca, K, and Mg purification was evaluated by purifying 10 replicates of a pooled human urine standard acquired from Innovative Research Inc., with sample volumes ranging from 0.3 to 1 mL. Urine Ca, K, and Mg concentrations were 87.2 ± 1.9 µg mL^{-1} (RSD = 2.2%), 1025 ± 42 µg mL^{-1}, (RSD = 4.1%), and 49.5 ± 1.4 µg mL^{-1} (RSD = 2.8%), respectively. Column yields were 97.4 ± 2.2%, 95.9 ± 2.6%, and 92.6 ± 3.8% (SD) for Ca, Mg, and K, respectively. The average $\delta^{41}K_{SRM\ 999c}$ value for 10 replicates was − 0.48 ± 0.03‰ (2SE, $N = 10$), with individual uncertainty of the sample measurement ranging from 0.01 to 0.06‰ (SD) (Fig. 3A). The average $\delta^{26}Mg_{ERM\ AE\text{-}143}$ value was + 3.10 ± 0.05‰ (2SE, $N = 10$), with individual errors ranging from 0.01 to 0.05‰ (SD) (Fig. 3B). The $\delta^{44/40}Ca_{SW}$ value for the urine standard was − 1.10 ± 0.09‰ (2SE, $N = 10$; Fig. 3C). Each urine standard was measured 2 to 4 times and has a similar isotopic composition to other urine samples, making it an ideal secondary standard for evaluating long-term reproducibility.

Isotopic analysis via CRC-MC-ICP-MS with syringe injection

High precision potassium isotope measurement in the collision cell mode has been shown to exhibit a pronounced effect from ion intensity mismatch between the sample and standard. This results in inaccurate $\delta^{41}K$ values when ion intensity matching falls outside of ± 1–5% [19, 23, 29], and the effect is highly dependent on daily tuning settings. To correct for this mismatch, Zheng et al. [29] proposed a mathematical correction method based on a single calibration curve, which allows for correction of ion intensity

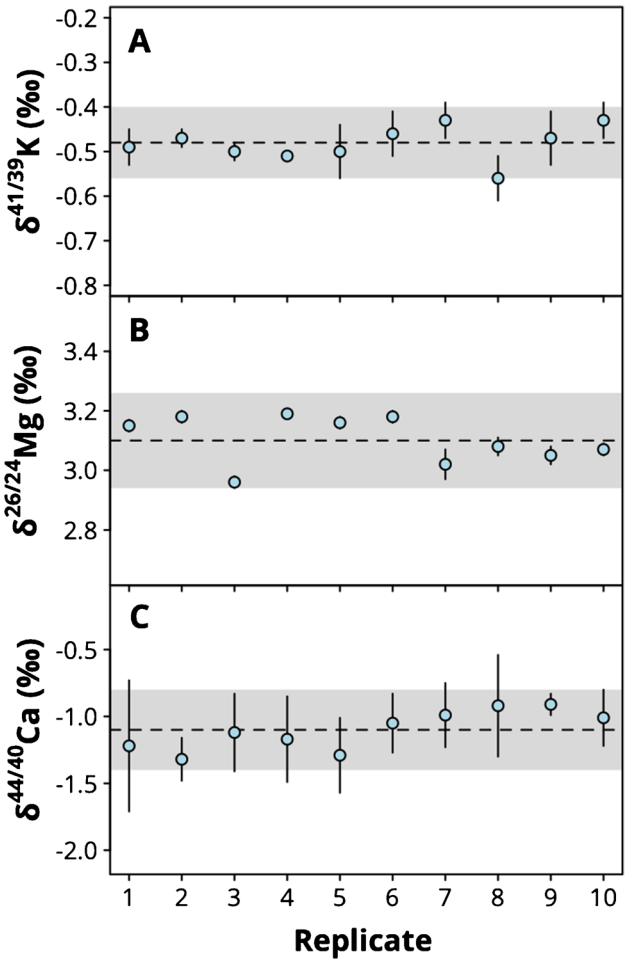

Fig. 3 Reproducibility of urine standard for K (**A**), Mg (**B**), and Ca (**C**) isotope ratios expressed as δ-values. Error bars correspond to 1SD of measurement replicates ($n = 2$–4). Gray area represents 2SE of the mean

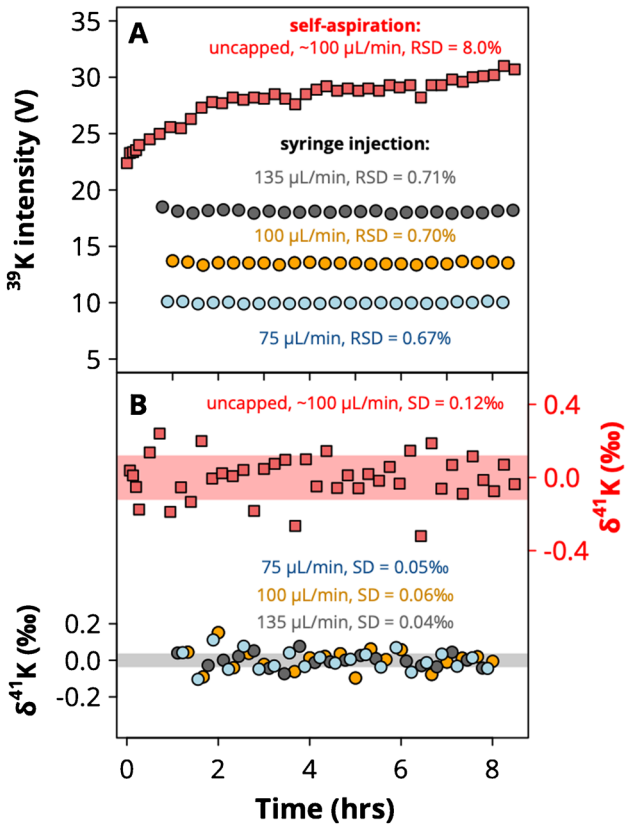

Fig. 4 Signal stability (**A**) and bracketed δ^{41}K values (**B**) at different flow rates. Uncapped solutions introduced via self-aspiration show drift to higher signal intensity with evaporation, as well as greater variance between analyses in intensity and isotope ratios. Syringe injection at different flow rates is consistently more reproducible in terms of signal intensity and isotope ratios. Note that greater initial signal intensity in self-aspiration data likely derives from higher-than-nominal nebulizer flow rate (>100 µL/min), not heightened sensitivity of self-aspiration relative to syringe injection.

mismatches up to 10%, resulting in intermediate precision of ≤ 0.05‰ (2SD) for δ^{41}K values.

Here, we present K isotope ratio measurements using syringe injection. This allows modification of syringe injection rates by ± 50% (50–150 µL min^{-1}) to achieve precise sample-standard intensity matching. A consistent injection profile of signal stability was maintained over a 9-h measurement sequence at flow rates of 75 µL min^{-1}, 100 µL min^{-1}, and 135 µL min^{-1} for K isotope ratio measurements, with an average RSD of 0.70% (Fig. 4A), when using the automated uncapping method to prevent sample evaporation during the sequence. For uncapped vials, the signal increased due to evaporation by more than 25% by the end of the sequence, resulting in an RSD of 8.0% (Fig. 4A). We note that this steady, large increase in signal intensity is observed for all analyses of uncapped beakers in our lab, regardless of autosampler model. The effect is most pronounced in solutions with high surface area-to-volume ratio. The uncapped run plotted in Fig. 4 is representative of typical conditions for an analytical sequence of uncapped PFA vials. The δ^{41}K values obtained via bracketing remained stable throughout the 9-h sequence for both capped and uncapped vials; however, uncapped samples exhibited 2–3 times higher variance ($SD_{uncapped} = 0.12$‰ vs. $SD_{capped} = 0.04$ to 0.06‰; Fig. 4B). Linear relationships were observed between total K intensity and flow rate ($R^2 = 0.999$; Fig. 5A), and between measured (unbracketed) δ^{41}K values and flow rate ($R^2 = 0.998$; Fig. 5B).

To closely match sample and standard intensities, quantification is performed with the isotope 2 software using an injection rate of 100 µL min^{-1} for all samples. Afterwards, the injection rate is defined by the user for each sample via the software to match the signal intensity of the bracketing standard. As mentioned above, the K isotopic composition of IAPSO SW measured against NIST 999c is in good agreement with the literature values (Table 4).

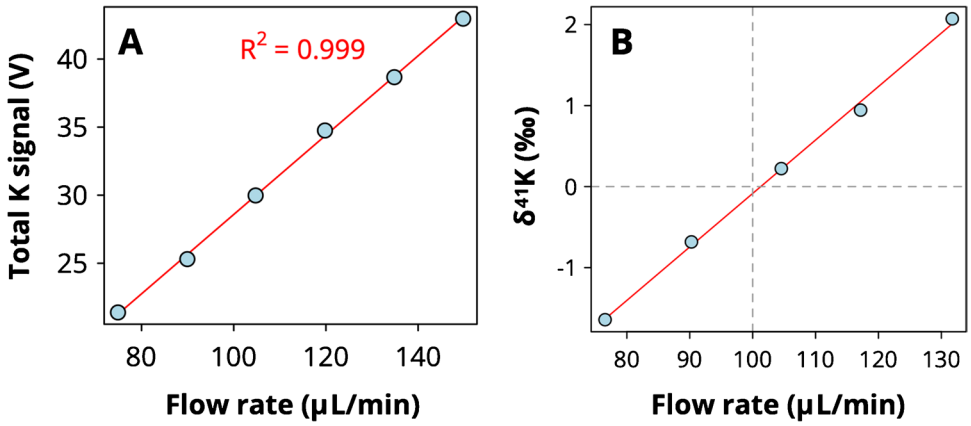

Fig. 5 Signal (**A**) and measured delta value (**B**) vs. syringe flow rate

Application to CKDu

Individuals with CKDu had significantly lower urine major ion concentrations than healthy individuals (21.7 vs. 81.0 mg Ca/L, $p=0.008$; 42.3 vs. 67.9 mg Mg/L, $p=0.05$; 462.0 vs. 626.0 mg K/L, $p=0.035$) (Fig. 6). Calcium isotope ratios were significantly higher in the urine of CKDu patients ($p=0.027$), whereas no significant differences were observed for Mg ($p=0.36$) or K ($p=0.47$) isotope ratios (Fig. 6). The Ca isotopic composition of all urine samples is negatively correlated with the Ca/Na ratio (Fig. 7), consistent with preferential reabsorption of lighter Ca isotopes via passive paracellular transport in the nephron driving urine Ca isotopic fractionation. Urine Ca/Na was also significantly lower in the CKDu group than the healthy group ($p=0.015$), whereas Mg/Na ($p=0.13$) and K/Na ($p=0.26$) showed no significant difference (Fig. 6).

The trend of lower ion content in urine from individuals with CKDu is consistent with previous findings of ion imbalance in CKD [22]. Clinically, CKDu often presents with mild to severe hypokalemia, hypomagnesemia, hyponatremia, and hypophosphatemia, which are typically suggestive of urinary electrolyte wasting [30–32]. This wasting reflects proximal tubular dysfunction. Under normal conditions, this nephron segment reabsorbs the majority of filtered electrolytes back into circulation. When tubular cells are damaged by toxins, heat stress, drugs, or inflammation, this reabsorptive capacity declines [33]. Mechanistically, tubular epithelial cells may develop mitochondrial dysfunction from repeated exogenous insults and shift from fatty acid oxidation toward glycolysis. This could result in reduced ATP levels, limiting the function of energy-dependent transporters, disrupting the osmotic and electrochemical gradients that usually drive passive reabsorption [17, 34].

The observation of heavier δ^{44}Ca values in CKDu urine samples alongside lower Ca excretion is consistent with renal reabsorption as the primary driver of isotopic variability. In this model, lower Ca excretion rates imply greater fractional Ca reabsorption, and the lower yield of residual, excreted Ca gives urine a correspondingly heavier isotopic composition. However, this observation is opposite in direction to previous work on pediatric CKD, which showed lighter δ^{44}Ca values in CKD patients than age-matched healthy controls [26]. In that study, lower δ^{44}Ca values converging toward the serum δ^{44}Ca composition were taken as evidence of bone resorption, which releases lighter Ca isotopes into serum and urine. The difference of trend in those pediatric CKD patients and our CKDu patients could thus reflect the difference in baseline bone mineral balance of children versus adult subjects, or possibly also a difference in renal physiology. In any case, because CKDu is characterized by predominant tubulointerstitial damage, electrolyte and ion imbalance may appear earlier and serve as a marker of disease progression before albuminuria or large declines in glomerular filtration rate (GFR).

Here we briefly consider possible explanations for the high urine δ^{44}Ca values observed in CKDu individuals. First, we note that short-term (days to months) intra-individual variation in urine δ^{44}Ca is typically much smaller than inter-individual δ^{44}Ca [27], suggesting that our data are indeed representative of a real physiological difference between groups. This is further supported by the fact that these urine samples are first morning void, which are most representative of whole-day average values [27].

We next consider isotopic effects not arising in the kidney. Bone is by far the largest Ca reservoir in the body (> 99%), and thus changes in bone mineral balance (BMB) are prone to cause large deviations in urine δ^{44}Ca values. Bones are isotopically lighter than soft tissue, meaning that times of net bone formation push urine δ^{44}Ca more positive while bone loss will push urine δ^{44}Ca values more negative [6, 18, 35, 36]. Renal dysfunction in CKD is associated with changes in BMB, with calcium wasting and phosphate retention leading to hyperparathyroidism and eventual bone loss [37, 38]. As

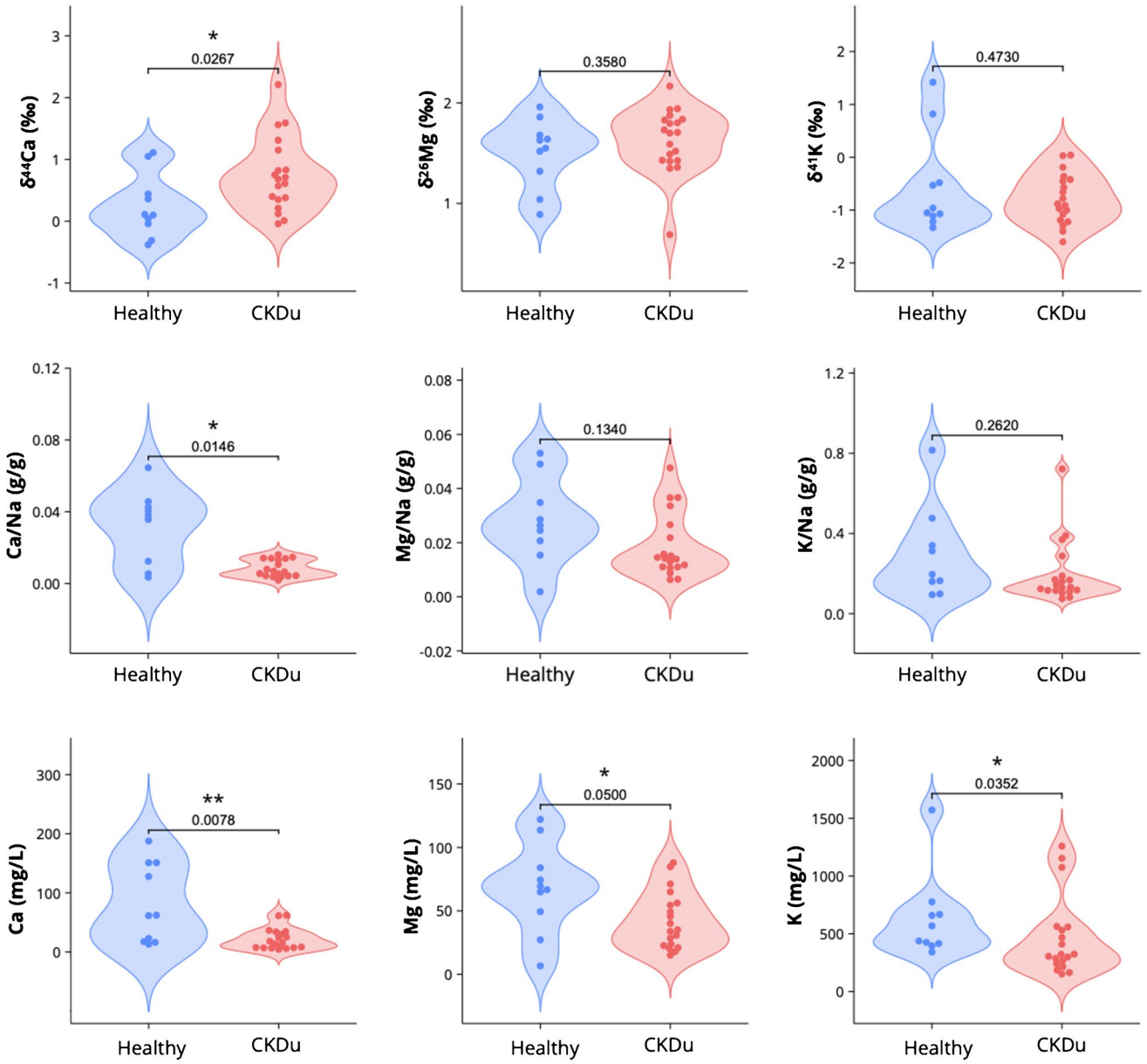

Fig. 6 Violin plots of elemental concentrations and isotopic ratios in healthy (blue, $n=10$) and CKDu (red, $n=20$) urine samples. *P* values denote significance of pairwise comparisons determined by t test or Wilcoxon rank sum test, depending on data normality

noted above, bone resorption tends to push serum and urine δ^{44}Ca values more negative, counter to what is observed here. Thus, we infer that BMB disruption is likely not the explanation for the observed high urine δ^{44}Ca values.

We also consider vascular calcification, which is common in CKD due to ion imbalance. One study noted a correlation between serum δ^{44}Ca values and markers of vascular calcification, with serum becoming isotopically heavier, supposedly due to mineral deposition of isotopically light Ca [39]. This could in theory push urine δ^{44}Ca values more positive, as observed in our data. However, we find this unlikely because (1) that study observed no such trend in urine samples (only serum) [39], and (2) the amount of Ca deposited in arteries and veins would be much smaller than the amount present in bone and the amount filtered by the kidney.

This leaves us to consider possible renal explanations for the ^{44}Ca enrichment in urine of individuals with CKDu. As noted before, preferential reabsorption of lighter Ca isotopes in the nephron pushes urine to isotopically heavier values. Changes in fractional Ca reabsorption thus are expected to result in urine δ^{44}Ca variability, following a Rayleigh distillation pattern [13]. Lower Ca concentrations coupled to higher δ^{44}Ca values are consistent with fractional Ca

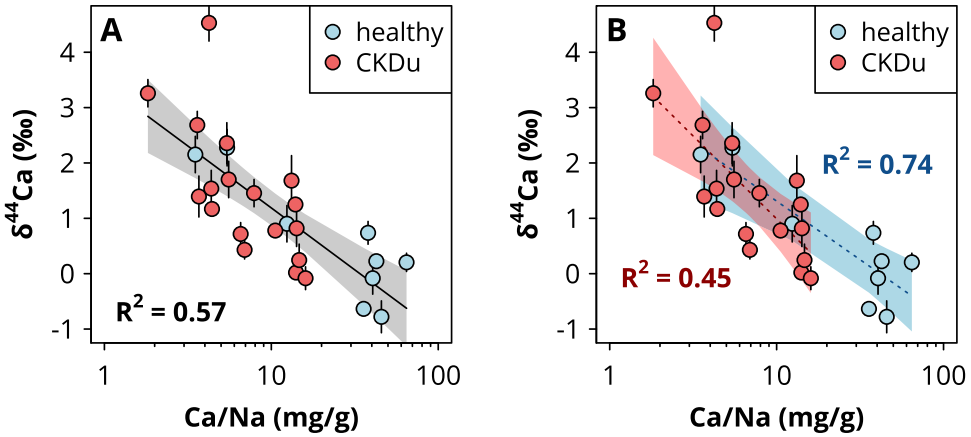

Fig. 7 Calcium isotope ratio versus Ca/Na in urine samples. Error bars are 2SD. Across both groups (healthy and CKDu), a correlation is observed between calcium isotope ratios and Ca/Na, with heavier isotopic compositions associated with lower relative Ca levels. This is consistent with isotopic fractionation imparted via passive paracellular reabsorption of Ca in the nephron, suggesting that the difference in the average isotopic composition between groups is driven by changes in ion reabsorption rates. Panels show single linear regression for all samples (**A**) and individual regression for healthy and CKDu individuals (**B**)

reabsorption in the kidney driving the observed trends, but imply greater Ca reabsorption in CKDu individuals than healthy controls, although serum Ca data are needed to validate this hypothesis. While this seems at odds with tubulointerstitial damage known to be prevalent in CKDu, we consider one potential reason for this observation: a change in the balance of passive versus active Ca reabsorption.

In healthy individuals, most Ca (up to ~ 90%) is reabsorbed via passive paracellular transport in the proximal convoluted tubule and thick ascending limb [16]. Passive transport is typically associated with isotopic fractionation in favor of the lighter isotope being more readily transported [40, 41], consistent with the observation that urine samples are isotopically heavy relative to serum [13, 18]. The remaining ~ 10% of Ca reabsorption occurs via active transport, in part modulated by parathyroid hormone (PTH). Active transport, in contrast, does not typically result in large isotopic fractionation [6, 41]—which is consistent with our lack of observed trend in δ^{41}K (Fig. 6), since K reabsorption is predominantly controlled by active transport in Na/K pumps [16] – meaning this portion of Ca reabsorption does not elevate urine δ^{44}Ca. Increased serum Ca due to diminished urinary Ca excretion tends to disfavor active Ca reabsorption via diminished PTH secretion [42]. Thus, individuals with CKDu could progress toward a ~ 100% passive Ca reabsorption regime in which the urine-serum isotopic fractionation is stronger than in healthy individuals. Such a scenario would imply not only higher δ^{44}Ca values in CKDu urine samples, but also a steeper δ^{44}Ca vs. Ca/Na slope due to a larger fractionation factor. This is potentially consistent with our data (Fig. 7A, B), but due to our small sample size, it is difficult to assess whether the CKDu and healthy control populations fall on a single fractionation line or distinct trends.

Further exploration of Ca elemental and isotopic trends in chronic kidney disease is needed to tease apart these potential mechanisms. Paired serum–urine isotopic analyses would be particularly powerful for quantifying isotopic effects of renal reabsorption. There is furthermore a need for coupling of novel isotopic tracers with traditional biomarkers to verify potential mechanistic explanations of isotope fractionation.

Conclusions

We have presented new methods for the efficient purification and isotopic analysis of major cations from biological samples. Using AG-50W-X8 and DGA resins in the prepFAST MC, we isolated purified K, Mg, Sr, and Ca fractions from synthetic and real urine solutions. This method enables automated four-element purification from a sample in ~ 3 h, which is comparable to many manual single-element chemistry approaches. With further optimization, Li can also be isolated from Na using the same method, but with a longer total runtime. Analysis of these solutions with a Nu *Sapphire* (CRC-)MC-ICP-MS was more efficient and stable when employing syringe injection using the micro*FAST* isotope 2 system. By modulating syringe injection rates, sample and standard solution intensities could be matched routinely to within 1–2%. Collectively, these methods enable much faster multi-isotopic analyses from single samples, lowering the barrier to multi-proxy studies and larger (even clinical-scale) datasets. We have demonstrated this potential with pilot analyses of urine from individuals diagnosed with chronic

kidney disease of unknown etiology (CKDu). These data suggest a change in Ca reabsorption for individuals with CKDu. Further work can compare these results to individuals with clinical CKD of various stages to assess differences in disease mechanism.

Supplementary Information The online version contains supplementary material available at https://doi.org/10.1007/s00216-025-06309-w.

Acknowledgements The authors thank Gary Dwyer for assistance with ICP-MS analyses at Duke.

Author contribution Conceptualization: RG, WS, MPF, AS, NJ, MAK; methodology: RG, WS; investigation: RG, WS, MPF, MAK; resources: MPF, MCDS, NJ; supervision: MPF, MAK; funding acquisition: AS, NJ, MAK; writing—original draft: RG, MAK; writing—review and editing: RG, WS, MPF, AS, NJ, MAK.

Funding Financial support for this work was provided by an NSF CAREER grant (award no. 2441483), an ACS Petroleum Research Fund grant (award no. 67594-DNI2), and start-up funds (Duke University) to MAK, as well as a Dean's Research Venture Fund (Nicholas School of the Environment, Duke University) award to MAK, NJ, and AS. This work was performed in part at the Duke University Shared Materials Instrumentation Facility (SMIF), a member of the North Carolina Research Triangle Nanotechnology Network (RTNN), which is supported by the National Science Foundation (award no. ECCS-2025064) as part of the National Nanotechnology Coordinated Infrastructure.

Data availability All new data generated in this study is provided in the main text and/or electronic supplementary materials.

Declarations

Ethical approval This study was conducted according to the guidelines of the Declaration of Helsinki and was approved by the Ethics Review Committee of the Faculty of Medicine, University of Ruhuna, Sri Lanka (Reference No. 2020.P.124, date: January 29, 2021). Informed written consent from each individual was obtained before participation.

Competing interests M. Paul Field and William Swenson are both employed by Elemental Scientific Incorporated. All other authors declare no competing interests.

References

1. Urey HC (1947) The thermodynamic properties of isotopic substances. J Chem Soc (Resumed) 562–581. https://doi.org/10.1039/JR9470000562.
2. Wiechert U, Halliday AN, Lee D-C, Snyder GA, Taylor LA, Rumble D. Oxygen isotopes and the Moon-forming giant impact. Science. 2001;294:345–8. https://doi.org/10.1126/science.1063037.
3. Paniello RC, Day JM, Moynier F. Zinc isotopic evidence for the origin of the Moon. Nature. 2012;490:376–9.
4. Misra S, Froelich PN. Lithium isotope history of Cenozoic seawater: changes in silicate weathering and reverse weathering. Science. 2012;335:818–23.
5. Farquhar GD, Ehleringer JR, Hubick KT. Carbon isotope discrimination and photosynthesis. Annu Rev Plant Physiol Plant Mol Biol. 1989;40:503–37. https://doi.org/10.1146/annurev.pp.40.060189.002443.
6. Skulan J, DePaolo DJ. Calcium isotope fractionation between soft and mineralized tissues as a monitor of calcium use in vertebrates. Proc Natl Acad Sci U S A. 1999;96:13709–13. https://doi.org/10.1073/pnas.96.24.13709.
7. Kędzior M, Garcia AK, Li M, Taton A, Adam ZR, Young JN, Kaçar B. Resurrected Rubisco suggests uniform carbon isotope signatures over geologic time. Cell Rep. 2022. https://doi.org/10.1016/j.celrep.2022.110726.
8. Wang RZ, Nichols RJ, Liu AK, Flamholz AI, Artier J, Banda DM, Savage DF, Eiler JM, Shih PM, Fischer WW. Carbon isotope fractionation by an ancestral rubisco suggests that biological proxies for CO_2 through geologic time should be reevaluated. Proc Natl Acad Sci U S A. 2023;120: e2300466120. https://doi.org/10.1073/pnas.2300466120.
9. Bizzarro M, Baker JA, Ulfbeck D. A new digestion and chemical separation technique for rapid and highly reproducible determination of Lu/Hf and Hf isotope ratios in geological materials by MC-ICP-MS. Geostand Newsl. 2003;27:133–45. https://doi.org/10.1111/j.1751-908X.2003.tb00641.x.
10. Roux P, Lemarchand D, Hughes HJ, Turpault M. A rapid method for determining boron concentration (ID - ICP - MS) and δ11 B (MC - ICP - MS) in vegetation samples after microwave digestion and cation exchange chemical purification. Geostand Geoanal Res. 2015;39:453–66. https://doi.org/10.1111/j.1751-908X.2014.00328.x.
11. Romaniello SJ, Field MP, Smith HB, Gordon GW, Kim MH, Anbar AD. Fully automated chromatographic purification of Sr and Ca for isotopic analysis. J Anal At Spectrom. 2015;30:1906–12.
12. Buisson M, Louvat P, Thaler C, Rollion-Bard C. High precision MC-ICP-MS measurements of 11 B/10 B ratios from ng amounts of boron in carbonate samples using microsublimation and direct injection (μ-dDIHEN). J Anal At Spectrom. 2021;36:2116–31.
13. Heuser A, Frings-Meuthen P, Rittweger J, Galer SJG. Calcium isotopes in human urine as a diagnostic tool for bone loss: additional evidence for time delays in bone response to experimental bed rest. Front Physiol. 2019;10: 12. https://doi.org/10.3389/fphys.2019.00012.
14. Grigoryan R, Costas-Rodríguez M, Vandenbroucke RE, Vanhaecke F. High-precision isotopic analysis of Mg and Ca in biological samples using multi-collector ICP-mass spectrometry after their sequential chromatographic isolation–application to the characterization of the body distribution of Mg and Ca isotopes in mice. Anal Chim Acta. 2020;1130:137–45.
15. Tacail T, Lewis J, Clauss M, Coath CD, Evershed R, Albalat E, Elliott TR, Tütken T. Diet, cellular, and systemic homeostasis control the cycling of potassium stable isotopes in endothermic vertebrates. Metallomics. 2023;15:mfad065.
16. Blaine J, Chonchol M, Levi M. Renal control of calcium, phosphate, and magnesium homeostasis. Clin J Am Soc Nephrol. 2015;10:1257–72.
17. Kolli RT, Gunasekara SC, Foster MW, Adduri S, Strasma A, Wyatt C, Konduru NV, De Silva MCS, Jayasundara N. The urinary proteome infers dysregulation of mitochondrial, lysosomal, and protein reabsorption processes in chronic kidney disease of unknown etiology (CKDu). Am J Physiol Renal Physiol. 2023;324:F387–403. https://doi.org/10.1152/ajprenal.00285.2022.
18. Eisenhauer A, Müller M, Heuser A, Kolevica A, Glüer C-C, Both M, Laue C, Hehn UV, Kloth S, Shroff R. Calcium isotope ratios in blood and urine: a new biomarker for the diagnosis of osteoporosis. Bone Rep. 2019;10:100200.
19. Albalat E, Télouk P, Balter V. Routine measurement of high-precision potassium stable isotope compositions using a

continuous-flow Neoma MC-ICPMS/MS. J Anal At Spectrom. 2024;39:2183–91.
20. Hill RC, Wang Z, Williams GD, Polyak V, Singh A, Kipp MA, Asmerom Y, Vengosh A. Reconstructing the depositional environment and diagenetic modification of global phosphate deposits through integration of uranium and strontium isotopes. Chem Geol. 2024;662: 122214.
21. Mahan B, Tacail T, Lewis J, Elliott T, Habekost M, Turner S, Chung R, Moynier F. Exploring the K isotope composition of Göttingen minipig brain regions, and implications for Alzheimer's disease. Metallomics. 2022;14:mfac090.
22. Hu Y, Chen X-Y, Xu Y-K, Teng F-Z. High-precision analysis of potassium isotopes by HR-MC-ICPMS. Chem Geol. 2018;493:100–8.
23. Nie NX, Grigoryan R, Tissot FL. High precision analysis of potassium stable isotopes using the collision/reaction cell Neoma MC-ICPMS/MS. J Anal At Spectrom. 2024;39:2038–48.
24. Blättler CL, Higgins JA. Testing Urey's carbonate–silicate cycle using the calcium isotopic composition of sedimentary carbonates. Earth Planet Sci Lett. 2017;479:241–51.
25. Heuser A, Schmitt A-D, Gussone N, Wombacher F. Analytical Methods. In: Calcium Stable Isotope Geochemistry. Berlin Heidelberg, Berlin, Heidelberg: Springer; 2016. p. 23–73. https://doi.org/10.1007/978-3-540-68953-9_2
26. Shroff R, Lalayiannis AD, Fewtrell M, Schmitt CP, Bayazit A, Askiti V, Jankauskiene A, Bacchetta J, Silva S, Goodman N. Naturally occurring stable calcium isotope ratios are a novel biomarker of bone calcium balance in chronic kidney disease. Kidney Int. 2022;102:613–23.
27. Tissot FL, Cleveland D, Grigoryan R, Kipp MA, Shafiee RT, Miaou E, Chunduri R, Melton H, Tacail T, Razionale D. Magnitude and timescales of Ca isotope variability in human urine: implications for bone mass balance monitoring. Metallomics. 2024;16:mfae050.
28. Ling M, Sedaghatpour F, Teng F, Hays PD, Strauss J, Sun W. Homogeneous magnesium isotopic composition of seawater: an excellent geostandard for Mg isotope analysis. Rapid Commun Mass Spectrom. 2011;25:2828–36. https://doi.org/10.1002/rcm.5172.
29. Zheng X-Y, Chen X-Y, Ding W, Zhang Y, Charin S, Gérard Y. High precision analysis of stable potassium (K) isotopes by the collision cell MC-ICP-MS "Sapphire" and a correction method for concentration mismatch. J Anal At Spectrom. 2022;37:1273–87.
30. Herrera R, Orantes CM, Almaguer M, Alfonso P, Bayarre HD, Leiva IM, Smith MJ, Cubias RA, Almendárez WO, Cubias FR. Clinical characteristics of chronic kidney disease of nontraditional causes in Salvadoran farming communities. MEDICC Rev. 2014;16:39–48.
31. Wijkström J, González-Quiroz M, Hernandez M, Trujillo Z, Hultenby K, Ring A, Söderberg M, Aragón A, Elinder C-G, Wernerson A. Renal morphology, clinical findings, and progression rate in Mesoamerican nephropathy. Am J Kidney Dis. 2017;69:626–36.
32. Wijkström J, Jayasumana C, Dassanayake R, Priyawardane N, Godakanda N, Siribaddana S, Ring A, Hultenby K, Söderberg M, Elinder C-G. Morphological and clinical findings in Sri Lankan patients with chronic kidney disease of unknown cause (CKDu): similarities and differences with Mesoamerican nephropathy. PLoS ONE. 2018;13: e0193056.
33. Chevalier RL. The proximal tubule is the primary target of injury and progression of kidney disease: role of the glomerulotubular junction. Am J Physiol Renal Physiol. 2016;311:F145–61. https://doi.org/10.1152/ajprenal.00164.2016.
34. Baker ML, Cantley LG. Adding insult to injury: the spectrum of tubulointerstitial responses in acute kidney injury. J Clin Invest. 2025. https://doi.org/10.1172/JCI188358.
35. Heuser A, Eisenhauer A. A pilot study on the use of natural calcium isotope (44Ca/40Ca) fractionation in urine as a proxy for the human body calcium balance. Bone. 2010;46:889–96.
36. Morgan JLL, Skulan JL, Gordon GW, Romaniello SJ, Smith SM, Anbar AD. Rapidly assessing changes in bone mineral balance using natural stable calcium isotopes. Proc Natl Acad Sci U S A. 2012;109:9989–94. https://doi.org/10.1073/pnas.1119587109.
37. Moe SM, Drüeke T, Lameire N, Eknoyan G. Chronic kidney disease–mineral-bone disorder: a new paradigm. Adv Chronic Kidney Dis. 2007;14:3–12.
38. Hill Gallant KM, Spiegel DM. Calcium balance in chronic kidney disease. Curr Osteoporos Rep. 2017;15:214–21. https://doi.org/10.1007/s11914-017-0368-x.
39. Dosseto A, Lambert K, Cheikh Hassan HI, Fuller A, Borst A, Dux F, Lonergan M, Tacail T. Calcium isotopes as a biomarker for vascular calcification in chronic kidney disease. Metallomics. 2023;15:mfad009.
40. Gussone N, Langer G, Thoms S, Nehrke G, Eisenhauer A, Riebesell U, Wefer G. Cellular calcium pathways and isotope fractionation in *Emiliania huxleyi*. Geology. 2006;34:625–8.
41. Higgins JA, Ramos DS, Gili S, Spetea C, Kanoski S, Ha D, McDonough AA, Youn JH. Stable potassium isotopes (41K/39K) track transcellular and paracellular potassium transport in biological systems. Front Physiol. 2022;13: 1016242. https://doi.org/10.3389/fphys.2022.1016242.
42. Evenepoel P, Bover J, Torres PU. Parathyroid hormone metabolism and signaling in health and chronic kidney disease. Kidney Int. 2016;90:1184–90.
43. Hu Y, Teng F, Helz RT, Chauvel C. Potassium isotope fractionation during magmatic differentiation and the composition of the mantle. JGR Solid Earth. 2021;126: e2020JB021543. https://doi.org/10.1029/2020JB021543.